Discharge-Based Pressure Sensors for High-Temperature Applications Using Three-Dimensional and Planar Microstructures

Scott A. Wright, *Member, IEEE*, and Yogesh B. Gianchandani, *Senior Member, IEEE*

***Abstract*—Two versions of microdischarge-based pressure sensors, which operate by measuring the change, with pressure, in the spatial current distribution of pulsed dc microdischarges, are reported. The inherently high temperatures of the ions and electrons in the microdischarges make these devices amenable to high-temperature operation. The first sensor type uses 3-D arrays of horizontal bulk metal electrodes embedded in quartz substrates with electrode diameters of 1–2 mm and 50–100-μm interelectrode spacing. These devices were operated in nitrogen over a range of 10–2000 torr, at temperatures as high as 1000 °C. The maximum measured sensitivity was 5420 ppm/torr at the low end of the dynamic range and 500 ppm/torr at the high end, while the temperature coefficient of sensitivity ranged from −925 to −550 ppm/K. Sensors of the second type use planar electrodes and have active areas as small as 0.13 mm^2. These devices, when tested in a chemical sensing system flowing helium as a carrier gas, had a maximum sensitivity of 9800 ppm/torr, a dynamic range of 25–200 torr, and a temperature coefficient of sensitivity of approximately −1412 ppm/K. [2008-0262]**

***Index Terms*—Plasma applications, plasma confinement, plasma measurements, plasma properties, pressure effects, sensitivity.**

I. Introduction

PRESSURE sensors that can operate at high temperatures have uses in numerous industrial sectors and have been used in gas turbine engines, coal boilers, furnaces, and machinery for oil/gas exploration. A number of optical approaches have been reported in the past, utilizing Fabry–Perot and other interferometers. Typically, these use an optically reflective cavity on the end of a fiber-optic cable; the cavity size changes with pressure, causing measurable interference changes in reflected light. A thin diaphragm is typically used as the reflective surface. Operating temperatures up to 800 °C have been achieved with sapphire membranes [1]. An interferometer-based sensor has also been fabricated inside a fiber-optic cable [2]. Another sensing technology uses Bragg gratings, which are photoinscribed into fibers and used to trace wavelength shifts caused by pressure and temperature changes at temperatures exceeding 350 °C and potentially over 1500 °C [3]. Piezoresistive pressure sensors with diaphragms made from silicon carbide [4], and more recently even Si [5], have been reported to operate at 600 °C. Sapphire membranes have also been used in this context [6].

Microdischarge-based pressure sensors can complement this portfolio by offering an electrical transduction and structural simplicity. Microdischarges are miniature localized plasmas (and may include, more generally, arcs or sparks) created in gas ambients between electrodes that, due to their size, demonstrate characteristics different from those of plasma regions created on a larger scale [7]. Microdischarges have been explored for applications in a variety of micro total analysis systems, including microscale optical emission spectroscopy systems for chemical sensing [8], [9]. Devices utilizing microdischarges are well suited for high-temperature operation as the electrons have average thermal energies exceeding 3 eV (34 815 K) [10] away from the cathode and small populations of very high energy electrons with thermal energies exceeding 400 eV near the cathode [11]. Ions have thermal energies exceeding 0.03 eV above ambient (644 K) in a 23 °C (269 K) ambient environment. These temperatures allow the species to be only minimally affected by a high- or low-temperature ambient, making it possible for microdischarge-based devices to operate at temperatures in excess of 1000 °C and potentially down to cryogenic temperatures. The targeted performance range for this work is 200 °C–1000 °C, but some baseline studies at room temperature are included. With regard to pressure sensors, microdischarge-based devices offer the possibility of structural simplicity and a direct electrical readout.

We report microdischarge-based pressure sensors that operate by measuring the change in spatial current distribution of microdischarges with pressure. The targeted pressure range is 10–2000 torr, as might be encountered in a variety of manufacturing applications. As gas pressure increases, the mean free path of ionized molecules is reduced, and consequently, the breakdown and discharge characteristics are altered. Microdischarge-based pressure sensors are fundamentally different than ion gauges, which are not effective at atmospheric pressure because the small mean free path of the created ions, i.e., 20–65 nm, makes them difficult to detect at the collector [12].

Manuscript received October 22, 2008; revised January 24, 2009. First published April 24, 2009; current version published June 3, 2009. This work was supported in part by the Engineering Research Centers Program of the National Science Foundation under Award EEC-9986866. Y. Gianchandani acknowledges support through the IR/D program while working at the National Science Foundation. Subject Editor C. Hierold.

The authors are with the Department of Electrical Engineering and Computer Science, University of Michigan, Ann Arbor, MI 48109 USA (e-mail: scottwri@umich.edu; http://www.eecs.umich.edu/~yogesh/).

Color versions of one or more of the figures in this paper are available online at http://ieeexplore.ieee.org.

Digital Object Identifier 10.1109/JMEMS.2009.2017110

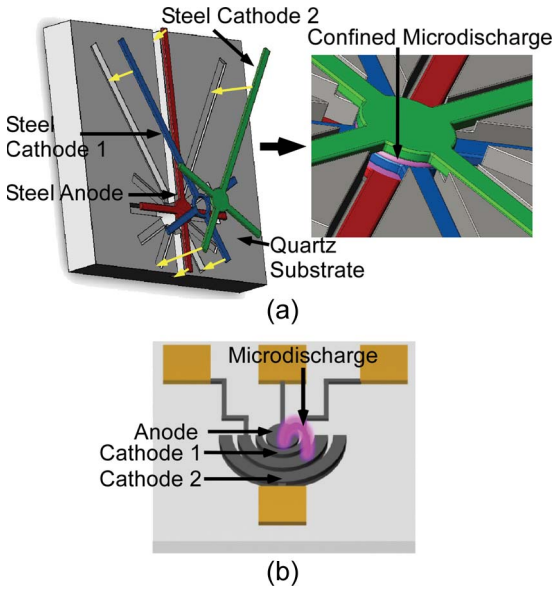

Fig. 1. Schematic of (a) a bulk foil sensor with electrodes above a quartz chip, illustrating placement, and the microdischarge chamber during operation, and (b) a planar sensor with microdischarge.

This paper describes two microdischarge-based microscale pressure sensor geometries—the bulk foil and the planar. Both geometries use multiple cathodes and provide a differential current readout. (Multiple anodes may also be used; however, anode current shows excessive pressure dependence because of the high mobility of electrons that dominate it [11]. This high sensitivity results in relatively small dynamic ranges, thereby limiting the utility of multianode configurations.) The first geometry, namely, the bulk foil, uses bulk metal foils in a stress-relieved two-cathode stack within a quartz substrate, and the second geometry, namely, the planar, uses planar thin-film metal electrodes on a Pyrex substrate.[1] The bulk foil sensors are designed for very high temperature operation, while the planar sensors, which use thin-film metals, are designed for conventional microfabrication. While this paper focuses on the performance of these devices in a nitrogen ambient, with appropriate encapsulation, they may be used in corrosive or liquid ambients. The operation of the devices and a current pulse circuit model is discussed in Section II. The fabrication processes and device designs are addressed in Section III. Experimental results from both sensor geometries are provided in Section IV.

II. Device Operation and Theoretical Considerations

The bulk foil sensor structure consists of several electrodes suspended over a cavity in a quartz chip (Fig. 1). Each electrode has a single lead for electrical contact and between one and three additional supports, which maintain the suspended position of the electrode. A microdischarge chamber exists in the center of the chip, in a through-hole, as shown in Fig. 1(a). A single disk-shaped anode electrode serves as the bottom of the chamber, while the center electrode is torus shaped, allowing the discharges to exist between the bottom anode and both cathodes. The top cathode is disk shaped as well, confining the discharges. The planar sensor structure consists of several patterned electrodes on a Pyrex substrate. A single circular planar anode is partially surrounded by concentric C-shaped cathodes, and microdischarges are created above the electrodes, as shown schematically in Fig. 1(b).

[1]Portions of this paper appear in conference abstract form in [13]–[15].

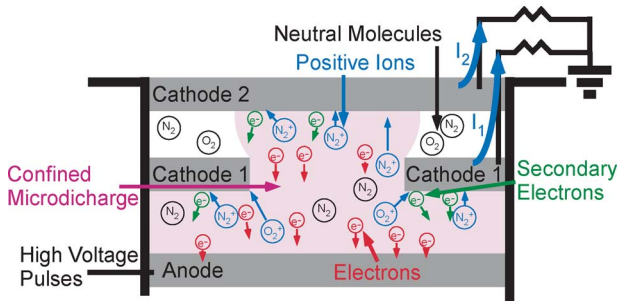

Fig. 2. Diagram of a microdischarge between a single anode and two cathodes in a bulk foil structure.

It is necessary to separately determine the current in two of the cathodes to determine the pressure. These current components are denoted as I_1 in the proximal cathode (cathode 1) and I_2 in the distal cathode (cathode 2). The differential current, expressed as a fraction of the total peak current, i.e., $(I_1 - I_2)/(I_1 + I_2)$, is treated as the sensor output. At low pressures, current favors the farthest cathode, while at high pressures, the opposite occurs. An important benefit of using a differential output that is expressed as a fraction of the total is that the exact magnitudes are less important than fractional changes.

The basic operation of a dc microdischarge in a bulk foil sensor is shown in Fig. 2, indicating electron and ion transport. The electrons are drawn toward the anode, whereas the positive ions are drawn to the two separate cathodes. Upon cathode impact, the energetic ions eject high-energy secondary electrons from the cathodes, which sustain the microdischarges by ionizing additional neutral molecules and continuing the breakdown process. High-energy ions are encountered in microdischarges at pressures higher than atmosphere as a result of the high power densities and voltage gradients encountered in the small gap spacing. The current in each cathode is composed of a combination of positive ions impacting the cathode from the microdischarge and secondary electrons ejected from the cathode upon ion impact. Further away from the cathodes, the current is carried primarily by the faster moving electrons.

A. Modeling Challenges

Power consumption and parasitic heating in the pressure sensors are controlled by using pulsed dc microdischarges, as opposed to constant dc discharges. The use of pulsed powering creates high-current pulse arcs (40–100 ns in duration), which initiate the microdischarges, as described by several authors [16]–[18]. The magnitudes of the current pulses show much greater sensitivity to pressure than the sustained dc current levels. However, while steady-state models exist for plasmas,

transient current pulses in microscale discharges have not been reported.

Microdischarges differ from macroscale plasmas in several aspects. In general, microdischarges can be sustained at higher pressures. They also experience much higher power densities, voltage gradients, and electric field strengths. Despite the high rate of collisions encountered at pressures approaching atmosphere, the electrons are in nonequilibrium, as they have much higher energies than the ions [7], [10], [11], [19]–[21]. When operating as glow discharges, microdischarge ionization is based on the creation of high-energy secondary electrons. A significant amount of these very energetic secondary electrons, i.e., "beam electrons," are accelerated to high velocities in the positively charged sheath region proximal to the cathode. This makes the models describing microdischarges complex, as the electron energy distribution function is highly non-Maxwellian [7], [11], [20], [21]. (The distribution function in macroscale discharges is typically assumed to be Maxwellian.) These differences between macroscale plasmas and microdischarges make the macroscale models [22] unrepresentative of the microscale, even in steady-state conditions. Multielectrode geometries, such as those proposed for this paper, pose additional challenges.

Several modeling techniques have been used to model steady-state microdischarges, most of which concentrate on cylindrically symmetric structures with a central hole through a metal–dielectric–metal sandwich stack [7]. Fluid models have been developed, which solve continuity, flux, and energy equations for separate species in the microdischarges [23]. A 2-D fluid model has been developed by Kushner [10], which takes into account both low-energy "bulk" and high-energy "beam" electrons and their position at various time steps. The model uses a Monte Carlo simulation to track the beam electrons, accounting for nonlocal plasma kinetics, collisionless heating, and nonequilibrium characteristics, which are pertinent to microdischarge operation. These are not considered in fluid models. Additional 1-D Monte Carlo models for steady-state microdischarges have also been developed [20], [21]. Kushner found the peak electric field near the cathode to be extremely high (over 80 kV/cm). The bulk electron temperatures are found to be 5.5–6.0 eV near the cathode and 2–3 eV between the electrodes. In an argon microdischarge, the ion densities are 2×10^{13} cm^{-3} at 50 torr and 1.8×10^{14} cm^{-3} at 625 torr, while densities up to 5×10^{16} cm^{-3} have been reported [24]. The development of a 3-D Monte Carlo simulation would be useful, given the multiple path lengths and spatially varying nonuniform fields in microdischarges.

B. Current Pulse Operation and Simulation

The current pulses in cathodes 1 and 2 of microdischarge-based pressure sensors are roughly approximated by a circuit model, which predicts the pulse profile in time as a function of discharge voltage. The pulse power source is represented by the discharging of a capacitor C, while the current pulse is represented as a series combination of an inductance L and a resistance R, as developed by Robiscoe *et al.* [25], [26]. A large shunt resistance R_s is used to allow a secondary current

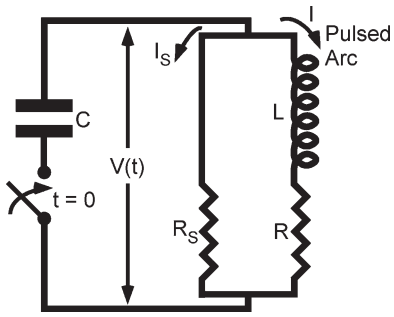

Fig. 3. Circuit model for high-current pulse arcs. The pulse power source is represented by the discharging of the capacitor C that is switched on at time $t = 0$. The current pulse is represented as a series combination of an inductance L and a resistance R along the current path. R_s is a shunt resistance, which allows a small amount of secondary current to flow during the main current pulse.

I_s to drain the capacitor, even if the pulse current I is zero. The pulse circuit model is shown in Fig. 3. As all of the circuit elements are passive, the relationships between voltage drops across the circuit elements result in a linear system of differential equations with constant coefficients. The solutions to these systems are damped trigonometric oscillations if the circuit rings, or exponentially decaying voltage profiles if the circuit is overdamped.

The circuit elements in the model can be determined using experimentally obtained pulse values. The pulse rise time, pulse duration, peak current, and pulse energy are all functions of the circuit element values and can thus be used to determine these values for the particular pulses encountered in cathodes 1 and 2 of the microdischarge-based pressure sensors. The pulse rise time is expressed as

$$t_r = (1 + 2\varepsilon)\frac{L}{R}\left(\ln\frac{1}{\varepsilon} - r\right) \tag{1}$$

where $\varepsilon = L/(CR^2)$ and $r = R/R_s$. The pulse duration is expressed as

$$t_p = [(1 + \varepsilon)RC]\,(1 - r). \tag{2}$$

The pulse peak current is

$$Ip = \frac{V_0}{R}\left[1 - \varepsilon \ln\left(\frac{1}{\varepsilon e}\right) - r\right] \tag{3}$$

where V_o is the initial applied voltage. The pulse energy is

$$Q = \frac{1}{2}\frac{CV_o^2/R}{(1 + r)(1 + \varepsilon r)}. \tag{4}$$

Fig. 4(a) shows the theoretical current pulses in cathodes 1 and 2 of a pressure sensor with electrodes spaced 50 μm apart, 1 mm in diameter, and 125 μm thick at a pressure of 200 torr. For cathode 1, the pulse rise time is 10 ns, the pulse duration, measured from initiation to the I_p/e time, is 50 ns, and the peak current is 235 mA. For cathode 2, the parameters are 20 ns, 40 ns, and 10.6 mA, respectively. Using these parameters and (1)–(3), the values for R, L, and C are obtained numerically for each cathode. Further refinement is possible by fitting to experimental results. The circuit elements for cathode 1 in the

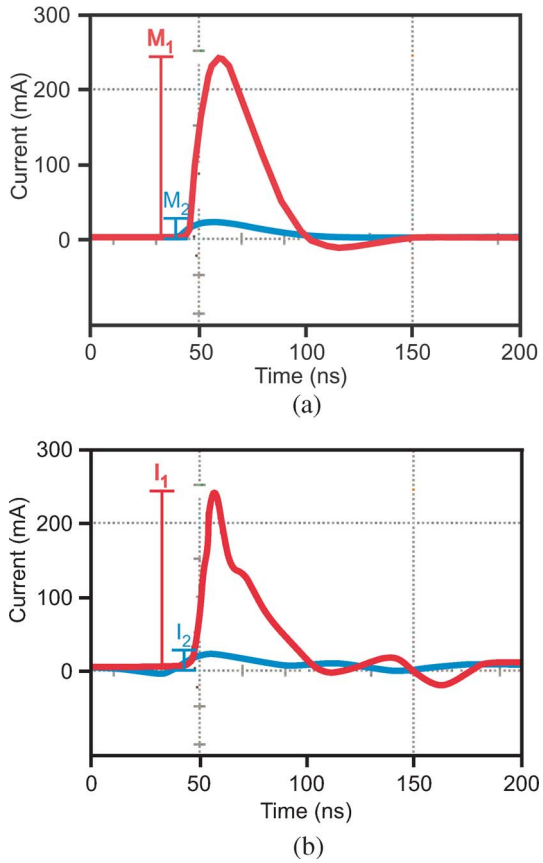

Fig. 4. (a) Modeled and (b) experimentally measured current pulses in cathodes 1 and 2 in a pressure sensor with electrodes spaced 50 μm apart, 1 mm in diameter, and 125 μm thick at 200 torr. The modeled current pulses in cathodes 1 and 2 are referred to as M_1 and M_2, respectively.

described sensor are found to be 2.6 kΩ, 25 μH, and 6.8 pF, respectively, and they are 48 kΩ, 600 μH, and 0.6 pF for cathode 2. The shunt resistance is simulated with a large impedance of 100 kΩ. The predicted current pulses as a function of time are determined through SPICE modeling. Similar analysis can be applied to determine the circuit elements for various pressure sensor configurations.

III. Fabrication

The bulk foil sensors, which are intended for operation at temperatures up to 1000 °C, use a quartz substrate. For the electrodes, #302 stainless steel is used for several reasons. Primarily, it is robust, inexpensive, easily machinable by microelectrodischarge machining and photochemical etching and has a sufficient secondary emission coefficient (i.e., 0.04 secondary electrons per incident 50-eV Na^+ ion [27]). Additionally, it is oxidation resistant at high temperatures and can be heated to 1420 °C before melting. Alternate refractory metals such as tungsten, molybdenum, and niobium oxidize at high temperatures in air, making them less desirable. Platinum, iridium, and platinum–rhodium are attractive options but are significantly more expensive than stainless steel.

The electrodes are lithographically patterned and etched from stainless-steel foil, using photochemical machining (Fig. 5) [28]. This process involves coating a thin sheet of metal

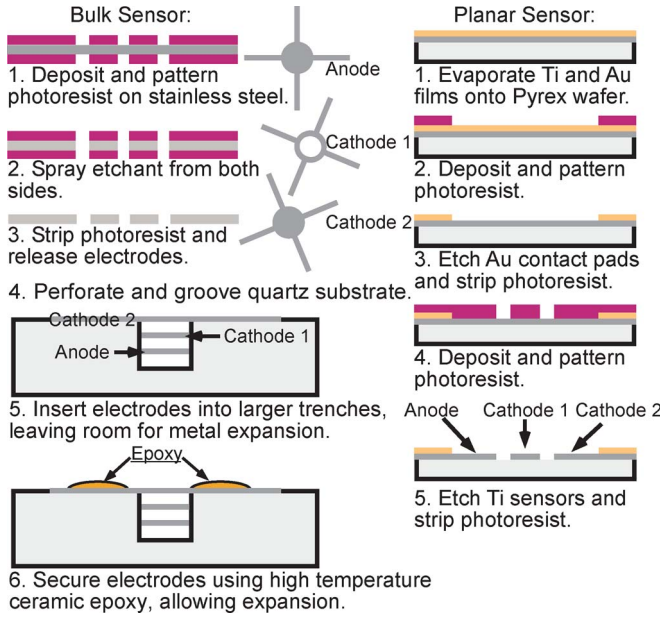

Fig. 5. Fabrication processes for bulk and planar sensors.

with photoresist, exposing the resist, and spraying the sheet with a chemical etchant to dissolve the exposed metal. The exposed metal is completely removed, leaving through-holes in the sheet, and the resist is stripped (Fotofab, Chicago, IL).

An arrangement that accommodates the expansion mismatch between electrodes and substrate is necessary as the electrodes are integrated into the substrate. Trenches of specified depths and a through-hole in the center are cut into the planar quartz substrate. Both mechanical and wet-etch processes can be used for this purpose. The electrodes are assembled into the trenches, with the circular portions located in the through-hole. The different depths between the various trenches specify the discharge gap spacing, as the electrodes lie flush with the bottom of the trenches. Ceramic epoxy holds the electrode lead and support arms in place, without adhering to the stainless steel. This allows the leads and supports to expand separately from the quartz chip and the ceramic epoxy without buckling. High-temperature-compatible wires are soldered to the electrodes, and the solder is encased in ceramic. This ceramic keeps the solder in position, so it maintains electrical contact, even at high temperatures.

The planar sensors, which are intended for operation at temperatures up to 200 °C, are even easier to fabricate (Fig. 5). The substrates are #7740 Pyrex glass wafers, which have a softening temperature of 820 °C. A Ti film (1 μm thick) and a Au film (500 nm thick) are thermally evaporated onto 500-μm-thick glass wafers without removing the wafers from vacuum. Thin-film titanium electrodes are used, as they have previously been utilized to create sustained microdischarges [29]. The contact pads are patterned on the gold layer by using photolithography, and the film is removed using Transene GE-8148 gold etchant, which does not etch titanium. The electrodes are then patterned in the titanium layer using photolithography.

The sensitivity, pressure dynamic range, and temperature dynamic range depend on a variety of dimensional parameters, including interelectrode spacing, electrode diameter, and cathode

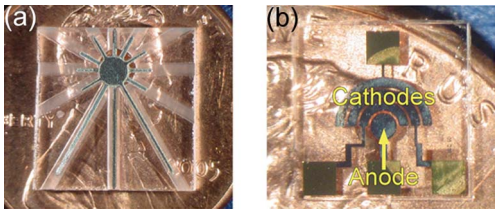

Fig. 6. (a) Bulk foil sensor with electrodes spaced 50 μm apart and 125 μm in thickness. (b) Planar sensor with three circular cathodes spaced 50 μm apart and 300 μm in width.

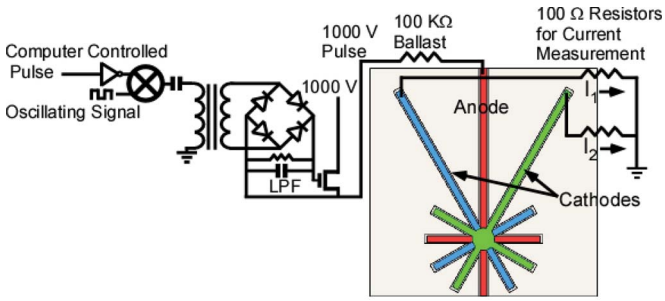

Fig. 7. Pulse-generating and readout circuitry used for sensor operation.

thickness. (Cathode thickness affects electrode spacing.) The anode/cathode spacing in these sensors is set to produce measurable results up to 1000 °C. (The sensors are designed to function with an applied voltage of 1000 V; altering the voltage results in different sensitivities.) A typical bulk foil design with electrodes spaced 50 μm apart, 1–2 mm in diameter, and 125 μm thick is shown in Fig. 6(a). These sensors have active areas of 0.8–3 mm^2 and are fabricated on 1-cm^2 chips.

The planar sensors used in this paper have three to seven cathodes, of which two are selected for the pressure measurement. The remaining are shunted to ground, and while they draw currents, they are not used in pressure measurement at this time. The cathodes are spaced 5–100 μm apart and are 5–300 μm in width. The sensors have active areas of 0.13–3 mm^2 and are fabricated on 0.25-cm^2 chips. A typical planar sensor design, with three circular cathodes spaced 50 μm apart and 300 μm in width, is shown in Fig. 6(b).

IV. Experimental Results

The bulk foil pressure sensors were fabricated and tested at various temperatures up to 1000 °C, measuring pressures between 10 and 2000 torr. Pulses, 1–20 ms in duration, were applied at a rate of 2–10 Hz to the anodes of the sensors with positive voltages between 700 and 1000 V. A computer-controlled single-ended transformer-coupled gate drive circuit created the pulses (Fig. 7). A current-limiting ballast resistor was used in series with the anode, and 100-Ω resistors were used in series with each cathode to measure current. The same circuitry powered the planar sensors. The pulses consumed between 168 μJ and 6 mJ each.

Current pulses were observed in each cathode. The current pulses were approximately 40–100 ns in duration, with amplitudes of 1.3 mA–2.85 A in the bulk foil sensors and 25 mA–2 A in the planar sensors, varying with temperature and pressure.

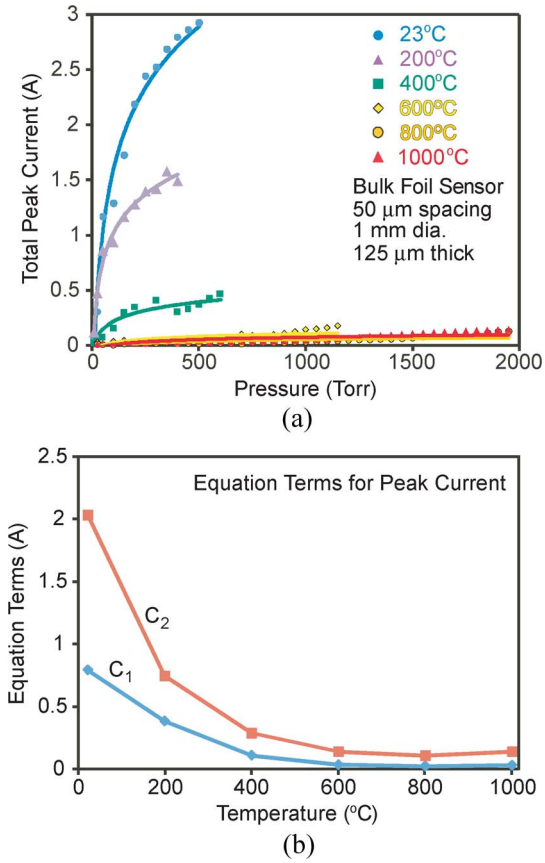

Fig. 8. Measured current pulse peak values. (a) Sum of the pulse currents in two bulk foil cathodes as a function of pressure and temperature. The empirical curves for each temperature are indicated by the solid lines. (b) Temperature trend for equation terms C_1 and C_2 in the peak current equation.

The experimentally obtained pulses in both cathodes are shown in Fig. 4(b). They demonstrated damped trigonometric current oscillations. The sum of the measured cathode current pulse peaks for a bulk foil device is shown in Fig. 8(a). At each temperature, this sum conforms to

$$I_{\mathrm{pk1}} + I_{\mathrm{pk2}} = C_1 \cdot \ln(p) - C_2. \tag{5}$$

The terms C_1 and C_2, determined by a least squares fit to the measured data in Fig. 8(a), are shown in Fig. 8(b) as a function of temperature. At temperatures greater than 600 °C, terms C_1 and C_2 saturate, indicating that the total cathode peak current becomes less dependent on temperature but remains dependent on pressure at higher operating temperatures.

A nitrogen-filled chamber with temperature and pressure control was used to test the bulk foil sensors. Fig. 9 shows fractional cathode currents, at 1000 °C, for a sensor design with electrodes spaced 50 μm apart, 1 mm in diameter, and 125 μm thick. As noted, the output of the sensor is the differential peak current between two cathodes, expressed as a fraction of the total peak current. The typical output for this sensor is shown in Fig. 10(a). Fig. 10(b) shows the typical output from a sensor design with electrodes spaced 100 μm apart, 1 mm in diameter, and 125 μm thick. The sensors demonstrate two regions of sensitivity (similar in some sense to touch-mode capacitive pressure sensors [30]). At low pressures, the response is highly

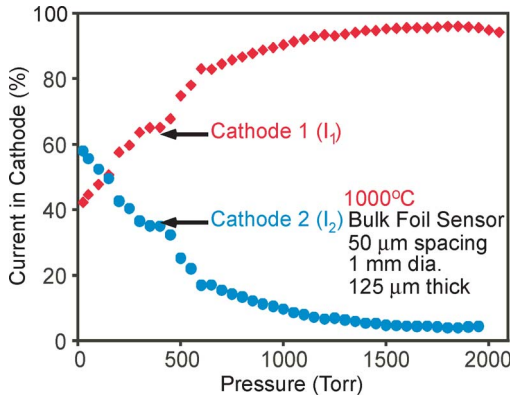

Fig. 9. Percentage of total current in the cathodes at 1000 °C in a bulk foil sensor with electrodes spaced 50 μm apart, 1 mm in diameter, and 125 μm thick.

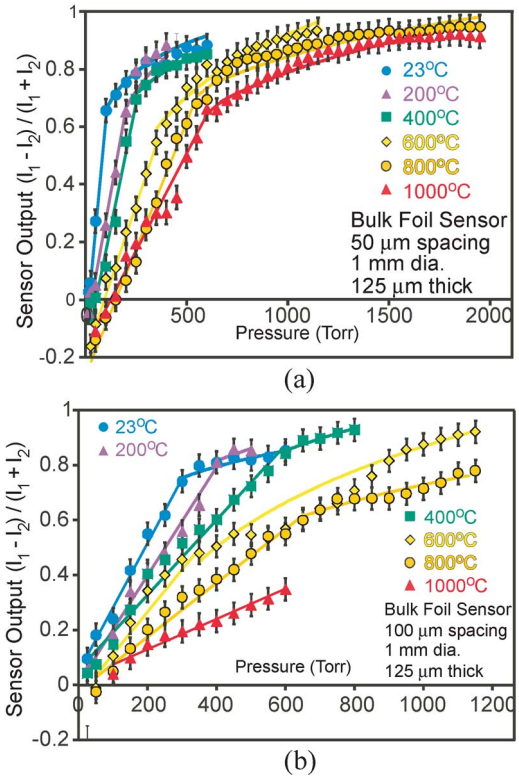

Fig. 10. Differential current output determined from the percentage of total current in bulk foil sensors with electrodes (a) spaced 50 μm apart and (b) spaced 100 μm apart, 1 mm in diameter, and 125 μm thick. Each data point is the average of 100 measurements. The two empirical curves per temperature are indicated by the solid lines.

linear, whereas at high pressures, it conforms to (5). The transition between these two regions rises from about 100 torr at room temperature to about 500 torr at 1000 °C. The average sensitivities in the low- and high-pressure operating regions of these sensors are shown in Fig. 11 as functions of temperature. One sensor design typically demonstrated the maximum lower pressure sensitivity, i.e., 5420 ppm/torr, as well as the maximum higher pressure sensitivity, i.e., 500 ppm/torr. Other design variations were also explored, and the typical results are listed in Table I. The minimum average temperature coefficient of sensitivity was −550 ppm/K.

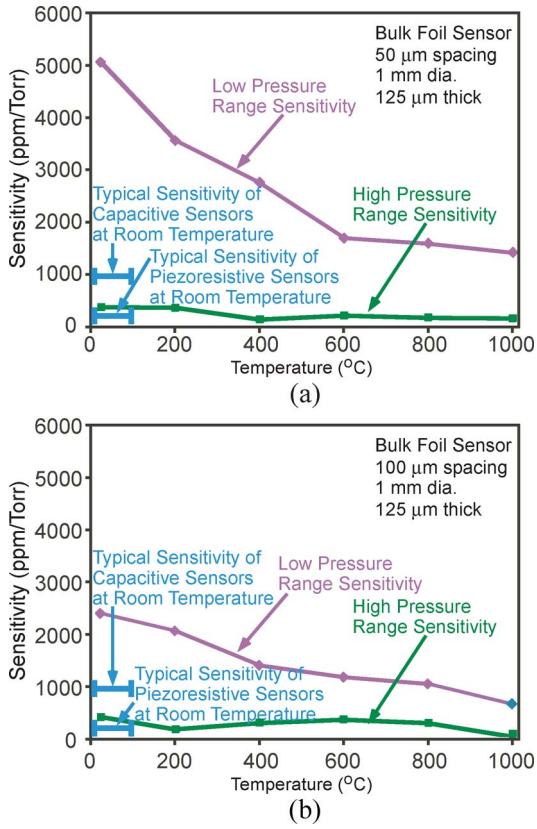

Fig. 11. Average sensitivities in both the low- and high-pressure ranges for the bulk foil sensors in Fig. 10(a) and (b) as functions of temperature.

TABLE I
TYPICAL PERFORMANCE OF FOUR DIFFERENT SENSOR DESIGNS, WITH THE HIGHEST PERFORMANCE IN EACH CATEGORY BEING IN BOLD

Sensor Parameters	Max Low Pressure Sensitivity (ppm/Torr)	Max High Pressure Sensitivity (ppm/Torr)	Dynamic Range (Torr)	Temp. Coeff. of Sensitivity (ppm/K)
Planar W=300 μm G =50 μm	**9,800**	**1,400**	175	-1,412
Bulk D=1 mm W=125 μm G=50 μm	5,060	380	**2,000**	-650
Bulk D=1 mm W=125 μm G=100 μm	2,170	220	1,150	**-550**
Bulk D=2 mm W=125 μm G=100 μm	**5,420**	**500**	900	-925

The planar sensors were tested in the context of a chemical sensing system, with an inert carrier gas (He) along with air and organic vapors. (Packaging these sensors with other devices and operating them concurrently demonstrated the ability of microdischarge-based sensors to function in systems, without disrupting the operation of other components.) Fig. 12 shows the fractional cathode current and differential output of a planar sensor packaged with other devices, as described earlier, with three cathodes spaced 50 μm apart and 300 μm in width. In

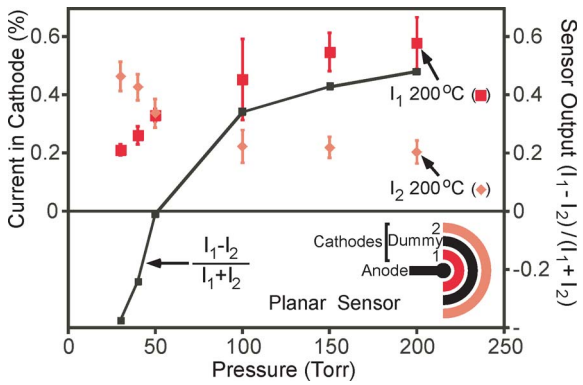

Fig. 12. Percentage of total current and differential current output in a planar sensor at 200 °C. The sensor has electrodes spaced 50 μm apart and 300 μm in width. Each data point is the average of 100 measurements.

this geometry, the intermediate cathode was grounded. Typical sensitivities were 9800 ppm/torr in the lower pressures, from 30–100 torr, and 1400 ppm/torr in the higher pressures, from 100–200 torr.

Sensitivity, dynamic range, and the temperature coefficient of sensitivity are the metrics used to compare microdischarge-based pressure sensor designs to one another and other pressure sensors. The performance of four different sensor designs, both planar and bulk foil, are shown in Table I, with the highest performance in each category being in bold. The data in the table represent typical operation of each sensor design.

V. Discussion

Several points concerning the sensor operation warrant a discussion, i.e., the temperature coefficients of sensitivity, the potential impact of electrode contamination, and the possibility of encapsulation.

The sensors demonstrate a negative temperature coefficient of sensitivity. For example, a sensor with electrodes spaced 50 μm apart, 1 mm in diameter, and 125 μm thick has sensitivities in the low-pressure region of 5060 ppm/torr at 23 °C and 1420 ppm/torr at 1000 °C. There are a number of possible contributors to the temperature coefficient of sensitivity, ranging from changes in the nature of the microdischarge to structural effects such as minor variations in electrode separation caused by expansion mismatch with the substrate. For comparison, typical piezoresistive and capacitive pressure sensors have sensitivities of 100 and 1000 ppm/torr, respectively, and temperature coefficients of sensitivity of $\pm$1000 to $\pm$5000 ppm/K [31], [32].

In nitrogen environments, coating of the electrode surfaces with contaminating thin films is not a primary concern in these sensors. In the past, microdischarges have been used to, and can unintentionally, coat electrode surfaces in reactive environments [33]. However, with discharges of sufficient energy, thin films are sputtered off the electrodes. This is demonstrated through the successful use of titanium electrodes, which form native titanium oxide layers in air. Radio-frequency discharges are also utilized to remove coatings [34].

In general, microdischarge-based pressure sensors should be calibrated for the gas environment in which they operate. To permit operation in variable environments that may additionally contain corrosive gases or even liquids, the pressure sensors can be encapsulated within a sealed cavity with a flexible diaphragm. The sealed cavity could contain pure nitrogen, helium, or other gas in which the discharges would be created. The external fluidic pressure would be transferred to the encapsulated gas through the diaphragm, taking advantage of the high sensitivity of the pressure sensor.

A logical progression for these sensors is the use of three, or more, cathodes to simultaneously enhance both sensitivity and dynamic range (albeit at the cost of increasing lead count at the circuit interface). This has been explored in a preliminary manner—devices with three or more cathodes were fabricated, but the signal output involved only two of the cathodes. The signal generated from two cathodes of a bulk foil device that had three cathodes spaced 100 μm apart, 3 mm in diameter, and 50 μm thick provides a relatively high sensitivity of 5000 ppm/torr but, not surprisingly, a compromised dynamic range of only 300 torr. Conversely, a planar design with five cathodes spaced 50 μm apart and 50 μm in width produces a uniform sensitivity of 2000 ppm/torr over 25–275 torr, when the signal is extracted from the two innermost electrodes.

The impact of electrode geometries is also worth investigating. In planar devices, for example, radial symmetry of the cathodes around a central anode seems to be a feature worth retaining. Experiments suggested that straight rectangular cathodes tend to compromise the sensitivity.

VI. Conclusion

The results indicate that microdischarge-based pressure sensors could be promising for use at high temperatures, at least up to 1000 °C, over the pressure range of 10–2000 torr. It is expected that these sensors can potentially operate at temperatures below room temperature and over larger dynamic pressure ranges. They provide an electrical readout, avoiding an intermediate transduction step, which can be convenient in some cases. The active areas for these devices are small enough to permit hybrid or monolithic integration with other components that constitute functional microsystems. The sensitivity achieved compares favorably with conventional piezoresistive and capacitive pressure sensors of comparable size. The absence of a diaphragm, which is commonly used in piezoresistive and capacitive pressure sensors, also provides natural tolerance for overpressure and, consequently, mechanical robustness. However, encapsulating the devices within a sealed cavity with a flexible diaphragm would permit them to be operated in a broad range of environments.

Acknowledgment

The authors would like to thank Prof. J. Foster for the discussions about dc discharges. The authors would also like to thank J. Park, M. Richardson, and W. Zhu for the assistance with microfabrication. The facilities used for this paper include the Michigan Nanofabrication Facility, University of Michigan, Ann Arbor. The findings do not necessarily reflect the views of the National Science Foundation.

REFERENCES

[1] R. Fielder, K. Stingson-Bagby, and M. Palmer, "State of the art in high-temperature fiber optic sensors," *Proc. SPIE*, vol. 5589, pp. 60–69, Dec. 2004.

[2] D. C. Abeysinghe, S. Dasgupta, H. E. Jackson, and J. T. Boyd, "Novel MEMS pressure and temperature sensors fabricated on optical fibers," *J. Micromech. Microeng.*, vol. 12, no. 3, pp. 229–235, Mar. 2002.

[3] T. Li, Z. Wang, Q. Wang, X. Wei, B. Xu, W. Hao, F. Meng, and S. Dong, "High pressure and temperature sensing for the downhole applications," *Proc. SPIE*, vol. 6757, pp. 675 706-1–675 706-7, Oct. 2007.

[4] A. Ned, R. Okojie, and A. Kurtz, "6H-SiC pressure sensor operation at 600 °C," in *Proc. Int. High Temperature Electron. Conf.*, Albuquerque, NM, 1998, pp. 257–260.

[5] S. Guo, H. Eriksen, K. Childress, A. Fink, and M. Hoffman, "High temperature high accuracy piezoresistive pressure sensor based on smart-cut SOI," in *Proc. IEEE Int. Conf. Micro Electro Mech. Syst.*, Tucson, AZ, 2008, pp. 892–895.

[6] S. Fricke, A. Friedberg, T. Ziemann, E. Rose, G. Muller, D. Telitschkin, S. Ziegenhagen, H. Seidel, and U. Schmidt, "High temperature (800 °C) MEMS pressure sensor development including reusable packaging for rocket engine applications," in *Proc. Micro-Nano-Technol. Aerosp. Appl. CANEUS*, Toulouse, France, 2006. 5p.

[7] R. Foest, M. Schmidt, and K. Becker, "Microplasmas, an emerging field of low-temperature plasma science and technology," *Int. J. Mass Spectrom.*, vol. 248, no. 3, pp. 87–102, Feb. 2006.

[8] V. Karanassios, "Microplasmas for chemical analysis: Analytical tools or research toys?" *Spectrochim. Acta B, At. Spectrosc.*, vol. 59, no. 7, pp. 909–928, Jul. 2004.

[9] B. Mitra and Y. B. Gianchandani, "The detection of chemical vapors in air using optical emission spectroscopy of pulsed microdischarges from two- and three-electrode microstructures," *IEEE Sensors J.*, vol. 8, no. 8, pp. 1445–1454, Aug. 2008.

[10] M. Kushner, "Modelling of microdischarge devices: Plasma and gas dynamics," *J. Phys. D, Appl. Phys.*, vol. 38, no. 11, pp. 1633–1643, May 2005.

[11] C. G. Wilson, Y. B. Gianchandani, R. Arslanbekov, V. Kolobov, and A. Wendt, "Profiling and modeling of DC nitrogen microplasmas," *J. Appl. Phys.*, vol. 94, no. 5, pp. 2845–2851, Sep. 2003.

[12] C. Edelmann, "Measurement of high pressures in the vacuum range with the help of hot filament ionization gauges," *Vacuum*, vol. 41, no. 7–9, pp. 2006–2008, 1990.

[13] S. A. Wright and Y. B. Gianchandani, "A harsh environment, multiplasma microsystem with pressure sensor, gas purifier, and chemical detector," in *Proc. IEEE Int. Conf. Micro Electro Mech. Syst.*, Kobe, Japan, 2007, pp. 115–118.

[14] S. A. Wright and Y. B. Gianchandani, "Microdischarge-based pressure sensors for operation at 1000 °C," in *Proc. Solid-State Sens. Actuators Microsyst. Workshop*, Hilton Head, SC, 2008, pp. 332–335.

[15] S. A. Wright and Y. B. Gianchandani, "A micromachined quartz and steel pressure sensor operating upto 1000 °C and 2000 Torr," in *Proc. IEEE Int. Conf. Micro Electro Mech. Syst.*, Sorrento, Italy, 2009, pp. 841–844.

[16] D. Staack, B. Farouk, A. Gutsol, and A. Fridman, "Characterization of a DC atmospheric pressure normal glow discharge," *Plasma Sources Sci. Technol.*, vol. 14, no. 4, pp. 700–711, Oct. 2005.

[17] H. Rahanman, B. Lee, I. Petzenhauser, and K. Frank, "Switching characteristics of microplasmas in a planar electrode gap," *Appl. Phys. Lett.*, vol. 90, no. 13, pp. 131 505-1–131 505-3, Mar. 2007.

[18] J. Choi, K. Matsuo, H. Yoshida, T. Namihira, S. Katsuki, and H. Akiyama, "Characteristics of a dc-driven atmospheric pressure air microplasma jet," *Jpn. J. Appl. Phys. 1, Regul. Pap. Short Notes*, vol. 47, no. 8, pp. 6459–6463, Aug. 2008.

[19] J. G. Eden and S.-J. Park, "Microcavity plasma devices and arrays: A new realm of plasma physics and photonic applications," *Plasma Phys. Control. Fusion*, vol. 47, no. 12B, pp. B83–B92, Nov. 2005.

[20] J. Choi, F. Iza, J. K. Lee, and C. Ryu, "Electron and ion kinetics in a DC microplasma at atmospheric pressure," *IEEE Trans. Plasma Sci.*, vol. 35, no. 5, pp. 1274–1278, Oct. 2007.

[21] Y. J. Hong, S. M. Lee, G. C. Kim, and J. K. Lee, "Modeling high-pressure microplasmas: Comparison of fluid modeling and particle-in-cell Monte Carlo collision modeling," *Plasma Process. Polym.*, vol. 5, no. 6, pp. 583–592, 2008.

[22] M. A. Lieberman and A. J. Lichtenburg, *Principles of Plasma Discharges and Materials Processing*. New York: Wiley, 1994.

[23] J. P. Boeuf, L. C. Pitchford, and K. H. Schoenbach, "Predicted properties of microhollow cathode discharges in xenon," *Appl. Phys. Lett.*, vol. 86, no. 7, pp. 071 501-1–071 501-3, Feb. 2005.

[24] M. Moselhy, I. Petzenhauser, K. Frank, and K. H. Schenbach, "Excimer emission from microhollow cathode argon discharges," *J. Phys. D, Appl. Phys.*, vol. 36, no. 23, pp. 2922–2927, Nov. 2003.

[25] R. T. Robiscoe and Z. Sui, "Circuit model of surface arcing," *J. Appl. Phys.*, vol. 64, no. 9, pp. 4364–4374, Nov. 1988.

[26] R. T. Robiscoe, A. Kadish, and W. B. Maier, II, "A lumped circuit model for transient arc discharges," *J. Appl. Phys.*, vol. 64, no. 9, pp. 4355–4363, Nov. 1988.

[27] S. G. Walton, J. C. Tucek, R. L. Champion, and Y. Wang, "Low energy, ion-induced electron and ion emission from stainless steel: The effect of oxygen coverage and the implications for discharge modeling," *J. Appl. Phys.*, vol. 85, no. 3, pp. 1832–1837, Feb. 1999.

[28] D. M. Allen, "The state of the art of photochemical machining at the start of the twenty-first century," *Proc. Inst. Mech. Eng. B, J. Eng. Manuf.*, vol. 217, no. 5, pp. 643–650, 2003.

[29] C. G. Wilson and Y. B. Gianchandani, "Silicon micromachining using *in situ* DC microplasmas," *J. Microelectromech. Syst.*, vol. 10, no. 1, pp. 50–54, Mar. 2001.

[30] S. T. Cho, K. Najafi, C. E. Lowman, and K. D. Wise, "An ultrasensitive silicon pressure-based microflow sensor," *IEEE Trans. Electron Devices*, vol. 39, no. 4, pp. 825–835, Apr. 1992.

[31] Y. Zhang and K. D. Wise, "Performance of nonplanar silicon diaphragms under large deflections," *J. Microelectromech. Syst.*, vol. 3, no. 2, pp. 59–68, Jun. 1994.

[32] *The MEMS Handbook*, 2nd ed. M. Gad-el-Hak, Ed. Boca Raton, FL: CRC Press, 2006.

[33] C. Schrader, P. Sichler, L. Baars-Hibbe, N. Lucas, A. Schenk, S. Draeger, K.-H. Gericke, and S. Buttgenbach, "Micro-structured electrode arrays: Plasma based sterilization and coating over a wide pressure range," *Surf. Coat. Technol.*, vol. 200, no. 1–4, pp. 655–659, Oct. 2005.

[34] A. Rizk and L. Holland, "Sputtering and chemical etching of carbon in a DC glow discharge," *Vacuum*, vol. 27, no. 10/11, pp. 601–604, 1977.

Scott A. Wright (M'09) received the B.S. degree in electrical engineering from the University of California, Los Angeles, in 2004, and the M.S. and Ph.D. degrees in electrical engineering from the University of Michigan, Ann Arbor, in 2006 and 2009, respectively, with a focus on circuits and microsystems.

He is currently a Postdoctoral Research Fellow with the Department of Electrical Engineering and Computer Science, University of Michigan. He was with Lockheed Martin Corporation, Sunnyvale, CA, and Bell Laboratories. His research interests include the study of plasma physics at the micrometer scale, microdischarges, and applications of microdischarges in micropumps, pressure sensors, and spectroscopic sensors.

Dr. Wright received the Armed Forces Communications and Electronics Association Fellowship for his work with microplasmas. He was the University of Michigan MIT Lincoln Laboratory Graduate Fellow for 2007–2008.

Yogesh B. Gianchandani (S'83–M'85–SM'04) received the B.S., M.S., and Ph.D. degrees in electrical engineering, with a focus on microelectronics and MEMS.

He is currently a Professor with the University of Michigan, Ann Arbor, with a primary appointment in the Department of Electrical Engineering and Computer Science and a courtesy appointment in the Department of Mechanical Engineering. He is temporarily with the National Science Foundation as the Program Director within the Electrical, Communication, and Cyber Systems Division. He was previously with the University of Wisconsin, Madison. He also held industry positions, working in the area of integrated-circuit design. His research interests include all aspects of design, fabrication, and packaging of micromachined sensors and actuators and their interface circuits. He has published approximately 200 papers in journals and conferences and is the holder of about 30 U.S. patents issued or pending. He was Chief Coeditor of *Comprehensive Microsystems: Fundamentals, Technology and Applications* (Elsevier, 2008). He serves as an Editor or a member of the Editorial Board for several journals.

Dr. Gianchandani was General Cochair for the IEEE/ASME International Conference on Micro Electro Mechanical Systems in 2002.